ELSEVIER

Polymer 40 (1999) 1553–1566

polymer

Effect of rubber functionality on microstructures and fracture toughness of impact-modified nylon 6,6/polypropylene blends: 1. Structure–property relationships

S.-C. Wong, Y.-W. Mai*

Center for Advanced Materials Technology, Department of Mechanical and Mechatronic Engineering, The University of Sydney, Sydney, NSW 2006, Australia

Received 16 December 1997; revised 24 April 1998; accepted 7 May 1998

Abstract

The effects of maleic anhydride (MA) content and its reactive functionality on the phase size and phase morphology of nylon 6,6/polypropylene (PP) blends were studied. The blends were obtained by simultaneous compounding of maleated styrene–ethylene–butylene–styrene block copolymers (SEBS) containing different amounts of MA, with nylon and PP. The microstructures were examined using cross-polarized transmission optical microscopy (TOM), scanning electron microscopy (SEM) and transmission electron microscopy (TEM). Both tensile and fracture properties of the maleated blends were reported and discussed in terms of the morphological features uncovered by these microscopic techniques. Tensile strength increased with MA-grafted SEBS content in the 75/25 nylon 6,6/PP blends but a reverse trend was observed in the 50/50 nylon 6,6/PP blends. It was thought that this was caused by the migration of the functionalized styrenic block copolymers from the PP phase to the dispersed nylon domains in the 50/50 nylon 6,6/PP blends. An optimized morphology was found when SEBS grafted with 0.74 wt% MA was blended with 75/25 nylon 6,6/PP. At this composition, SEBS inclusions were dispersed uniformly in the continuous nylon matrix and thin layers of SEBS molecules also existed at the nylon-PP interface. The latter gave a morphology similar to a core-shell rubber modified structure (i.e. SEBS shell and PP core) and imparted the highest fracture toughness to this blend with an optimal combination of tensile strength and ductility.

Keywords: Blends; Nylon 6,6; SEBS

1. Introduction

Toughening of nylon and isotactic polypropylene (PP) using styrenic block copolymers has received considerable attention in recent years [1–13]. Styrenic or other block copolymers are purposely designed to contain phase-segregated hard and soft segments with the primary function as a thermoplastic elastomer. Use of functionalized block copolymers such as maleic anhydride (MA) grafted styrene–ethylene–butylene–styrene (SEBS) to affect morphological control and thence toughening in multiphase polymer mixtures has become the main thrust in polymer blends research recently [1–5,7–13]. There is much scientific and commercial value in designing a suitable architecture whose micro-domains can provide reactive interfaces for bi-phase polymers during melt processing. Of equal importance is the effective use of the designed copolymers in enhancing the fracture toughness, by promoting interfacial adhesion and controlling microstructures of ternary blends. It is well known [1–4,7–13] that functionalized styrenic block copolymers are promising candidates as an interfacial agent, whose non-polar olefinic mid-block can penetrate the PP domains and whose grafted anhydride groups exhibit a strong affinity for the amine-end groups on nylons. Recent works by Gonzalez-Montiel et al. [11–13] and Oshinski et al. [9,10] have shown that by altering the level of functionality in commercially available SEBS-*g*-MA, drastic changes in morphology and performance of nylon/PP blends can be obtained. It was observed [1–3,11–13] that the maleated copolymers served both as a compatibilizer and an elastomer in the nylon 6/PP blends. Rösch [8] and Rösch and Müllhaupt [7] have suggested a core-shell morphology in PP/nylon 6 blends with a continuous PP matrix, wherein nylon formed the rigid core encapsulated by an elastomeric shell given by the functionalized block copolymers. In addition, Gonzalez-Montiel et al. [14] also reported that the PP domain size generally decreased as the MA content increased in nylon 6/PP-*g*-MA blends,

* Corresponding author.

0032-3861/98/$ - see front matter
PII: S0032-3861(98)00363-2

while Duvall et al. [15] showed decreased PP domain size, as the volume fraction of MA-grafted PP increased in the 75/25 nylon 6,6/PP blends. However, fracture properties were not studied by the previous authors [14,15] in these nylon/PP blends. With rubber modified nylon/PP blends even less is understood about the effect of the level of rubber functionality on the microstructures and fracture properties. It is the objective of this paper to elaborate on some of these observations and to investigate the dependence of the phase morphology and fracture toughness on the level of functionality in a class of rubber-modified nylon 6,6/PP blends.

The microstructures of nylon 6,6/PP blends containing SEBS-*g*-MA are rather complex. An in-depth understanding of the optimised morphologies for maximum toughness is much desired when formulating novel blends with a good balance of tensile strength and fracture toughness. The formula to toughen nylon 6 using SEBS-*g*-MA could not be directly translated into that to toughen nylon 6,6 [10], for example, due to fundamental differences in chemical nature between the two polyamides. It is essential to investigate independently the structure–property relationship of each system of blends to achieve the desired fracture–mechanical properties. In this study, the microstructures of nylon 6,6/PP blends modified by SEBS-*g*-MA were examined using transmission optical microscopy (TOM), scanning electron microscopy (SEM) and transmission electron microscopy (TEM).

To understand the fracture properties of multiphase polymers, it is often useful to first investigate the deformation mechanisms under an applied uniaxial load. Generally speaking, poor interfacial strength (adhesion) leads to poor ductility but not vice versa. Particle debonding from the matrix prior to yielding could lead to poor tensile strength and low failure strain. Conversely, interfacial strength that exceeds the yield stress of the second phase particles can give rise to good tensile strength but not necessarily high failure strain. How global deformation occurs depends not only on particle–matrix interfacial strength but also on the local failure (stress–strain) criteria, which are intrinsic functions of particle size [9–11,15–17,7–19], elastic modulus [17–19], volume fraction [9,10,13,20,21], debonding mechanism [22,23] and testing conditions (i.e. strain rate and temperature). Debonding of large, second-phase particles may create critical-size flaws, resulting in premature failure. However, flaw formation is more likely to be suppressed as the particle size decreases. In this work, the effect of particle failure micromechanisms on the fracture toughness properties of the nylon 6,6/PP blends was studied using TOM, equipped with a cross polariser.

2. Experimental work

2.1. Materials

Materials were dry blended, simultaneously, at weight ratios of 0/100, 12.5/87.5, 25/75, 50/50, 75/25, 87.5/12.5 and 100/0 nylon 6,6/PP, plus 20 wt% SEBS-*g*-MA. For 75/25 and 50/50 nylon 6,6/PP blends, a mixture of non-maleated SEBS and maleated SEBS was used at 5 different levels. After proportionally blending maleated with non-maleated SEBS, a homogeneous mixture [9–13] of copolymers could be obtained at MA levels of 0, 0.37, 0.74, 1.47 and 1.84%. The maleated SEBS is expected to be grafted to the nylon phase via an imide linkage during reactive compounding. The rest of the SEBS component remains non-grafted. Nylon 6,6 resin (Vydyne 21) was supplied by Monsanto Chemical Company and PP (Propathene GSE52) was obtained from ICI, Australia. The triblock copolymer SEBS (Kraton G1652) and its maleated version (Kraton F1901X) were supplied by Shell Chemical. The MA content of the Kraton FG1901X was 1.84%. For the non-maleated SEBS, molecular weight of the styrene block was given [9,11,12] as 7000 and that of the ethylenelbutylene block was 37 500. Molecular weights for the maleated copolymer were not available from the manufacturer.

2.2. Experimental procedure

Compounding of the nylon 6,6/PP blends with 20 wt% SEBS-*g*-MA was carried out using a high shear-rate twin-screw extruder (Wemer and Pfieiderer ZSK 30) at a temperature range of 260°C–280°C, varying with the nylon content, followed by injection molding (BOY 22S Dipronic). All materials were dried at 60°C in a vacuum oven at reduced pressure prior to compounding and in a regular oven prior to injection molding into 6 mm-thick Izod bars, which were machined into single-edge notched bend (SENB) specimens, and 3 mm-thick tensile specimens (ASTM D638 type I).

Tensile tests were conducted according to ASTM D638, using an Instron Model 5567 computer-controlled testing machine and the tensile strength, elastic modulus and ductility were simultaneously recorded. The crosshead speed was 10 mm min^{-1} at room temperature. Five specimens of each blend composition were tested.

The *J*-integral fracture toughness for the specimens was determined using a deeply notched three-point bend specimen with a span-to-width ratio, $S/W = 4$ ($L = 82$ mm, $W = 126$ mm, and thickness, $B = 5.8$ mm). Initial notches were introduced mid-way along the specimen lengths using a diamond saw. Pre-cracks were made by inserting a fresh razor blade into the machined slots and the crack-to-width ratio, a/W, was limited to 0.50–0.65 in all tests. The specimens were then loaded at a crosshead speed of 5 mm min^{-1} at room temperature. After unloading, the specimens were put in a bath of liquid nitrogen for at least 15 min and then fast-fractured. The amount of stable crack growth, Δa, was measured using a stereo-microscope (WILD Heerbrugg) and the *J*-integral fracture resistance, J_R, was determined from:

$$J_R = \frac{2U}{Bb} \tag{1}$$

where U is the area under the load *versus* load point–displacement curve, and b is the ligament length. The data for the J_R-curve were best-fitted to a power law relationship in accordance with ASTM Standard E813-89:

$$J_R = C_1 \Delta a^{C_2} \quad (2)$$

where C_1 and C_2 are curve-fitting parameters. The fracture initiation toughness, J_C, was determined by the intersection of the J_R–Δa curve with the blunting line solution at 0.2 mm offset, as recommended by ASTM E813-89, although there are uncertainties in the interpretation of this J_C value [24].

To investigate the SEBS particle debonding micromechanism, ~5 μm thick samples were cut from the necked region of fractured tensile specimens and examined with an optical microscope (Leica Leitz DMRXC) equipped with a cross polariser. Undeformed samples were also microtomed from the SENB specimens for observation under transmitted light. Fractographic examinations of the SENB J_C specimens with varying nylon 6,6/PP ratios were carried out on gold–palladium coated samples with a Philips 505 SEM.

TEM analysis was employed to identify the microstructures and morphology of 75/25 nylon 6,6/PP blends as a function of the MA content. Techniques involving TEM have been shown to be a powerful tool in capturing the microstructures of multiphase polymer mixtures in recent years [2–5,7–14]. The major challenge of employing TEM analysis for polymers lies in the highly sophisticated sample preparation procedures necessary to obtain ultra-thin specimens with adequate transparency and contrast when exposed to a ~120 kV electron beam. Samples were trimmed to rectangular blocks, perpendicular to the flow direction using a razor blade. The tips of the blocks were further trimmed into smaller surfaces (0.3 × 0.3 mm) for cryo-sectioning. Ultra-thin sections were slowly (0.2 mm s^{-1}) sliced off at about − 40°C, from the surface parallel to the flow direction, using a glass knife coated with tungsten in a Reichert Ultracut S microtome. A droplet of 2.3 mol sucrose in phosphate-buffered saline was used to pick up the cut sections, dry, from the edge of the glass knife and the sections were then placed on copper grids for rinsing in distilled water for at least 30 min before staining. Two staining techniques were used and compared in this work to reveal the phase dispersions and morphology of the second phase particles. The grids with the first set of sections were stained in 2% phosphotungstic acid mixed with 2% benzyl alcohol for 0.5 h [25] to reveal the nylon phase, leaving the rubber and PP particles unstained. The second set of specimens were vapour stained by RuO_4 prepared in situ, following Trent et al. [26], for 0.5 h unless otherwise specified. It was found that ultra-thin sections of the 75/25 blend containing non-maleated SEBS alone crumbled at the knife edge due to poor interfacial adhesion, which rendered the cryo-sectioning of 60 nm-thick sections extraordinarily difficult.

3. Morphology of nylon 6,6/PP blends containing 20wt% SEBS-*g*-MA

3.1. Effect of MA content on PP domain size of 75/25 nylon 6,6/PP blends modified by SEBS-g-MA as revealed by SEM fractography

Fig. 1 shows a schematic of the fracture surface divided into a stable crack growth region (A) and a fast cryo-fractured surface region (B) for SENB specimens tested for J_C. Note that as the crack advances, a curved crack front normally develops due to the prevalent plane strain constraint in the centre of the crack plane. The crack growth region A of 75/25 nylon 6,6/PP blends modified by SEBS-*g*-MA at different MA levels is given in Fig. 2. Particle size dependence of the PP phase on MA-grafted SEBS content in a nylon-dominant matrix at a fixed copolymer weight fraction (20 wt%) is clearly illustrated in these photomicrographs. Lack of interfacial adhesion causes large interfacial cracks to be formed on fracturing in the non-maleated SEBS modified blend (Fig. 2a). The fracture surface appears rather brittle. There is no compatibility between the nylon phase and the dispersed PP particles. Addition of 0.37%-maleated SEBS drastically alters the particle size of the second phase in the nylon/PP blend (Fig. 2b). Extensive ductile tearing in the crack growth region is clearly discernible. A further increase in MA-grafted SEBS content reduces the dispersed particle size (Fig. 2c) until the second-phase inclusions are no longer distinguishable from the SEBS-grafted nylon matrix (Fig. 2d–e). Close examination (Fig. 3) of the cryo-fractured region B at 1.47% MA level, however, reveals voiding and particle debonding which cannot be seen in Fig. 2d. A phase-separated morphology at 1.84% MA is only visible at higher magnification (Fig. 4). Under low temperature and fast loading rate, the yield stress of the rubber modified nylon matrix is increased and ductile tearing is suppressed on fracturing. The materials deform by voiding and second-phase particle debonding, as noted on the cryo-fractured surfaces.

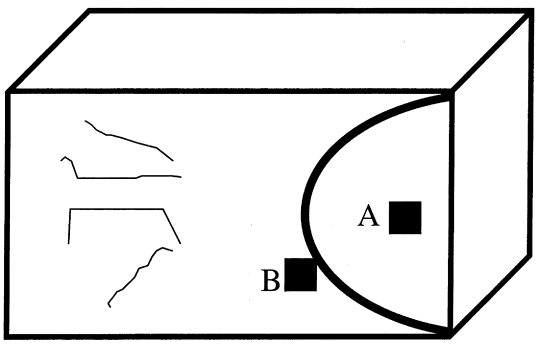

Fig. 1. A schematic fracture surface for SEM examination of nylon 6,6/PP blends containing SEBS-*g*-MA.

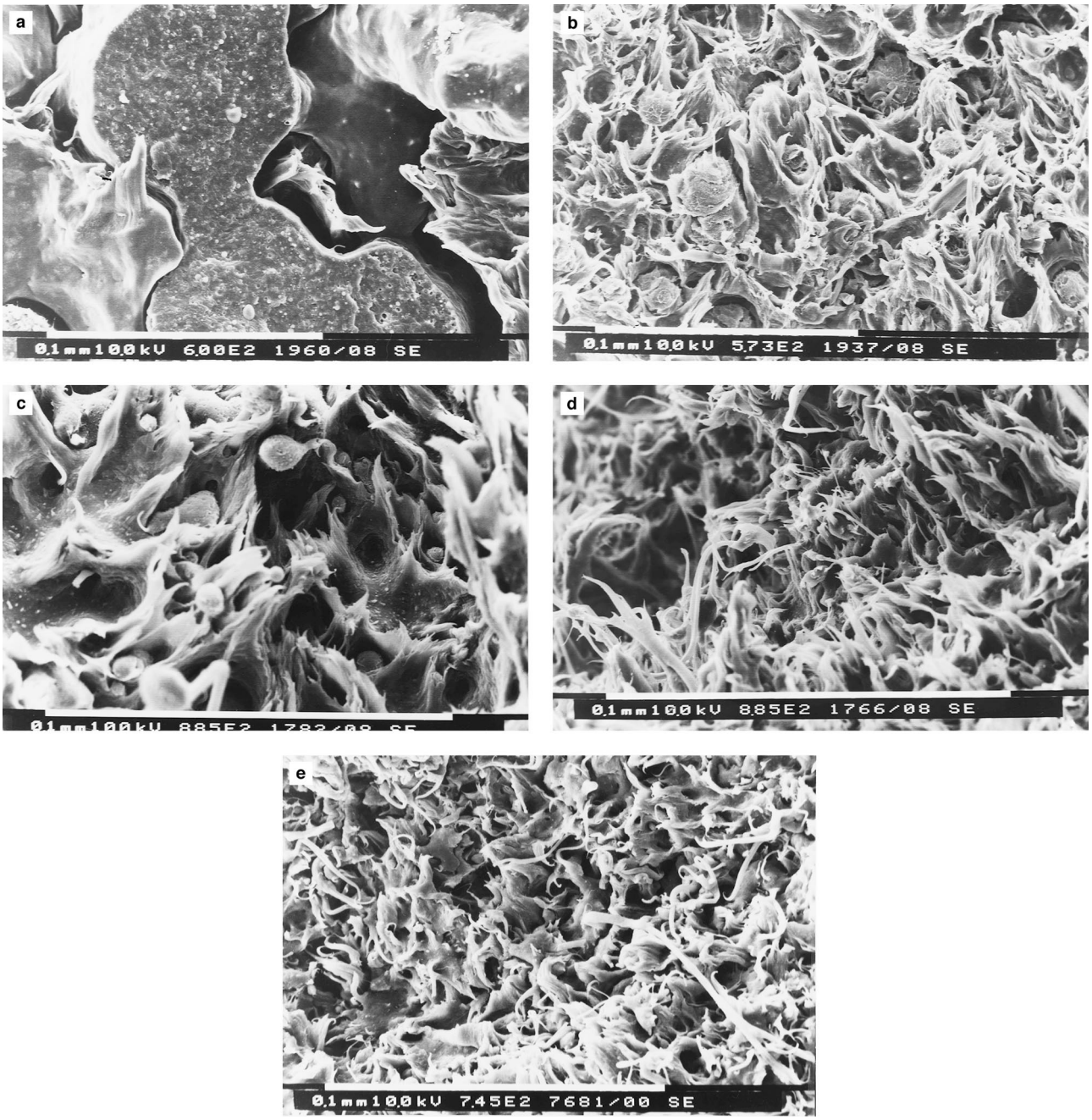

Fig. 2. SEM photomicrographs of 75/25 nylon 6,6/PP blends containing 20 wt% SEBS-*g*-MA: (a) 0% MA; (b) 0.37% MA; (c) 0.74% MA; (d) 1.47% MA; and (e) 1.84% MA.

3.2. Effect of MA content on second-phase domain size of 50/50 nylon 6,6/PP blends modified by SEBS-g-MA as revealed by SEM fractography

Fig. 5 shows a series of SEM fractographs of nylon 6,6/PP blends containing 20 wt% SEBS-*g*-MA as a function of nylon/PP ratio. The MA content was fixed at 1.84 wt%. For the seven different blend compositions, it is clear that there exists a smooth phase transition from a nylon-continuous morphology (Fig. 5a–b, Fig. 4) to a PP-continuous structure (Fig. 5c–f). Careful examination of the fractographs shows that phase inversion occurs at 50/50 nylon 6,6/PP blends, as characterised by the more intense drawing of the PP matrix material. The nylon 6,6/PP ratio at which phase inversion occurred resembles that reported by Gonzalez-Montiel et al. [11,12] on nylon 6/PP blends, containing functionalized block copolymers. This phase inversion as revealed by SEM fractographs at 50/50 ratio is corroborated by drastic reductions in tensile strength and elastic modulus, when the continuous nylon phase changes

Fig. 3. An SEM photomicrograph of 1.47%-maleated 75/25 nylon 6,6/PP blend containing SEBS-*g*-MA in Zone B of Fig. 1.

to a continuous PP phase, as reported elsewhere [27]. Fig. 6 shows different particle size and interfacial morphology for the 50/50 nylon 6,6/PP blends modified by SEBS-*g*-MA at different MA levels. With non-maleated SEBS (Fig. 6a) the 50/50 blend shows an extremely coarse morphology, suggesting a highly incompatible system in the absence of rubber functionality. Massive interfacial debonding is found. Finely dispersed SEBS particles are loosely embedded in the PP phase, whereas the nylon domains remain clear of any SEBS inclusions. Addition of 0.37%-maleated SEBS reduces the size of protruded nylon-grafted SEBS particles that are more uniformly distributed but clearly debonded, as shown in Fig. 6b. This confirms insufficient interfacial adhesion between the block copolymers and the dispersed nylon-grafted SEBS particles without sufficient MA content. Dispersed non-grafted SEBS particles are primarily located in the PP phase in these blend compositions. With increased MA-grafted SEBS content, it is clear that the nylon particle size gradually decreases (Fig. 6c–d, Fig. 5c). The results show consistency with the 75/25 nylon 6,6/PP blends, although the dispersed phase in this case is the nylon-grafted SEBS particles and PP forms the continuous phase.

Fig. 4. An SEM photomicrograph of 1.84%-maleated 75/25 nylon 6,6/PP blend containing SEBS-*g*-MA in Zone B of Fig. 1.

3.3. Micromorphology revealed by TOM and TEM for 75/25 nylon 6,6/PP blends modified by SEBS-g-MA

Equipped with a cross polariser, microtomed thin samples (≈5 μm) under TOM show dispersed phase of various sizes in 75/25 nylon 6,6/PP blends containing SEBS-*g*-MA. Fig. 7a displays the micro-morphology of dispersed phase in 0.37%-maleated SEBS modified blend, as revealed under transmitted light. Large particles abound in the nylon-continuous phase. Compared with Fig. 7b, a TOM photomicrograph of 0.74%-maleated SEBS blend, it is clear that the latter exhibits a much finer texture in second-phase dispersion, where the particles are relatively small and uniformly distributed in a nylon-continuous matrix. A TOM photomicrograph of a blend with the highest MA content, 1.84%, is given in Fig. 7c. A relatively coarse texture, coupled with extensive dark agglomerations of dispersed phase precipitated on the thin section, is noted under polarised light. To verify how exactly the second phase/phases are dispersed in the nylon-rich matrix, a more sophisticated assessment of the microstructures afforded by TEM techniques is essential.

TEM photomicrographs of the ternary blends of 75/25 nylon 6,6/PP at a fixed weight fraction of combined MA-grafted and non-grafted SEBS are shown in Figs 8–11. Two staining techniques for ultra-thin sections are compared and their respective photomicrographs are juxtaposed to give a clear understanding of the second phase dispersions in the continuous nylon matrix. Generally, PTA stains the nylon phase in the ternary blends; SEBS appears light grey, leaving PP unstained. The ability of RuO_4 to preferentially stain the component phases, however, varies with the phase morphology induced by different levels of reactive functionality associated with the thermoplastic elastomer. Phase contrast is generally good between SEBS and PP; SEBS is stained particularly well at the nylon–PP interface. But the nylon phase may or may not be stained in the presence of RuO_4, depending on the interpenetrating network formed with maleated SEBS. RuO_4 can stain SEBS dark and nylon phase light grey or grey; PP phase appears light grey or unstained, as reported in the nylon 6/PP/SEBS-*g*-MA system [11–13]. However, intimate interaction between the grafted SEBS and nylon 6,6 facilitates formation of ‘sub-microstructures’, wherein phase contrast between grafted SEBS and nylon 6,6 becomes less discernible. This results in a coarse texture of both SEBS and nylon 6,6 phases, which are only stained grey in RuO_4, even given a prolonged period of time. Simultaneous comparison of both PTA- and RuO_4-stained samples is therefore necessary to distinguish and identify the microstructures and morphology of nylon 6,6/PP/SEBS-*g*-MA blends.

With 0.37% MA in the blend matrix, dispersion of PP domains is not optimized in the nylon-continuous phase. The PTA-stained section is shown in Fig. 8a. Both oblong and elongated PP particles in the nylon phase, inside which smaller but well distributed SEBS spheres are finely

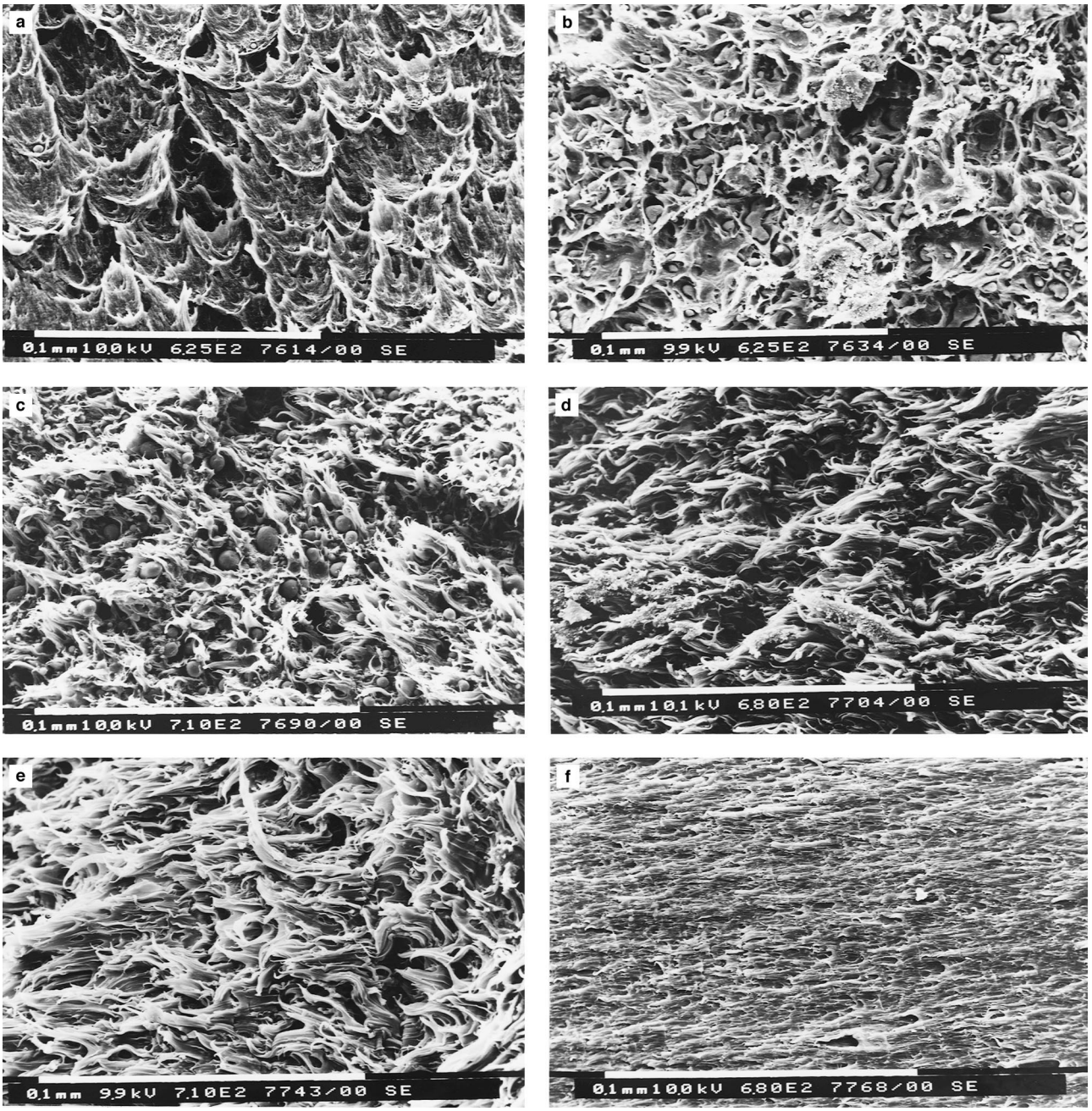

Fig. 5. SEM photomicrographs of nylon 6,6/PP blends containing 20 wt% SEBS-*g*-MA as a function of nylon 6,6/PP ratios: (a) 100/0; (b) 87.5/12.5; (c) 50/50; (d) 25/75; (e) 12.5/87.5; and (f) 0/100. MA content remains unchanged at 1.84%.

embedded, can be observed. Verification of SEBS dispersions in a RuO_4-stained section (Fig. 8b) also reveals that a substantial portion of SEBS is located at the nylon 6,6–PP interface and large PP particles are surrounded by non-uniform fringes of SEBS, which are stained dark by RuO_4. SEBS particles in the nylon phase are also stained dark consistent with the microstructures revealed in PTA-stained sections. A RuO_4-stained section at a lower magnification (Fig. 8c) displays irregular-shaped PP domains, wherein discrete SEBS inclusions are located at the interface and in the nylon-continuous phase. Nylon and PP phases appear unstained, even given a prolonged period of time (15 h). As shown in Fig. 9a, the 0.74%-maleated blend shows enhanced dispersion of PP in the nylon phase, which is illustrated by spherical PP inclusions of various sizes unstained by PTA. More interestingly, the non-uniform, thick layers of RuO_4-stained SEBS (Fig. 9b) diminish at the nylon–PP interface when the MA-grafted SEBS proportion is increased (MA content = 0.74%). Yet a relatively uniform dark fringe surrounding the light PP inclusions is still noticeable, confirming the presence of SEBS-rich molecules at the interface. While sub-micron SEBS

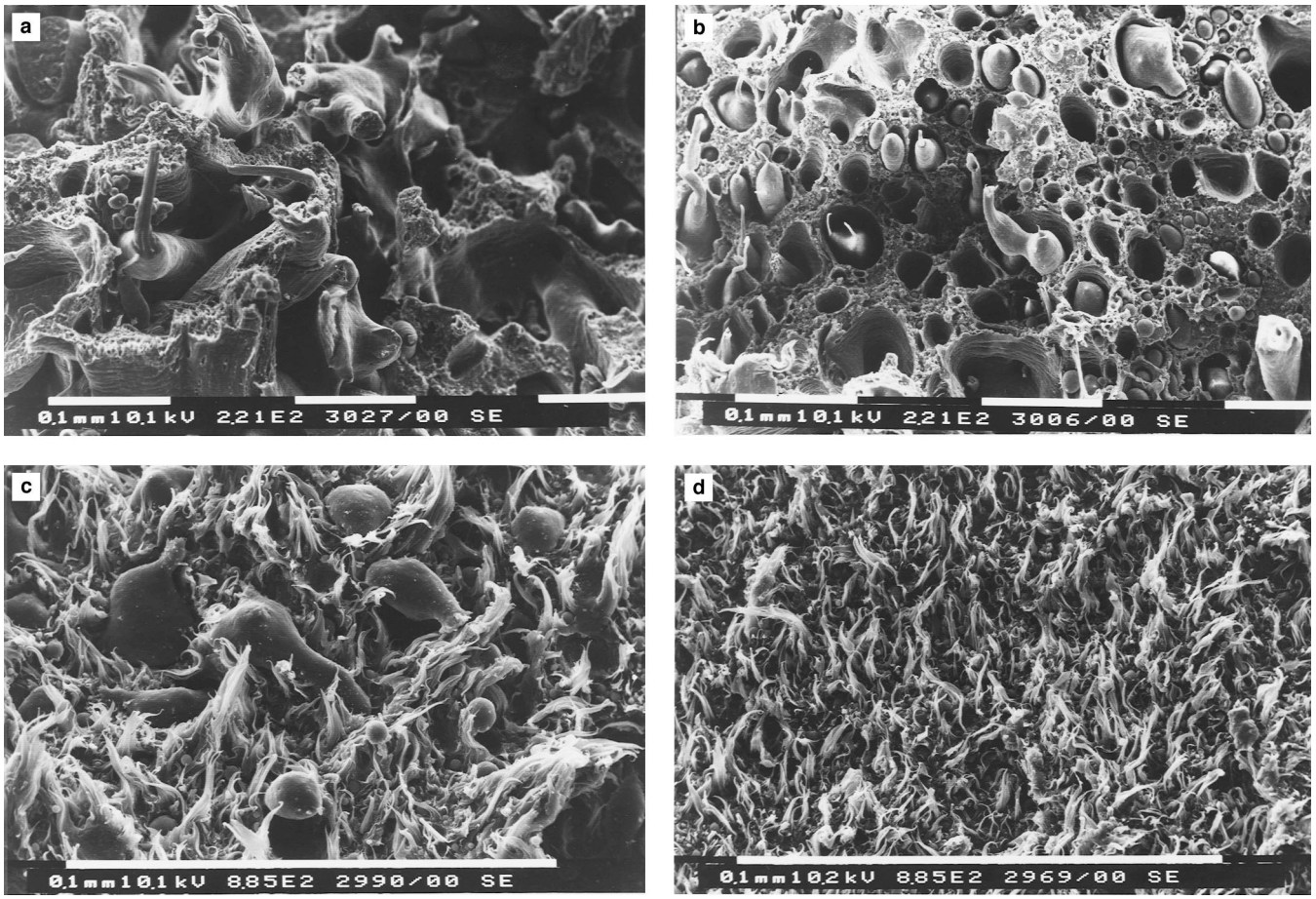

Fig. 6. SEM photomicrographs of 50/50 nylon 6,6/PP blends containing 20 wt% SEBS-*g*-MA: (a) 0% MA; (b) 0.37% MA; (c) 0.74% MA; and (f) 1.47% MA.

particles are evidently better distributed in the nylon phase (Fig. 9a), they are only vaguely distinguishable when stained with RuO_4 (Fig. 9b) because the SEBS phase becomes submerged in the nylon phase and both phases appear equally stained by this strong oxidising agent. The well dispersed SEBS particles, with diameters less than 1 μm, are believed to effectively toughen the nylon continuous phase [16,20,28–32]. The results confirm that SEBS-*g*-MA acts concomitantly as a toughening agent in the nylon phase and a compatibiliser for the nylon 6,6–PP interface.

Figs. 10 and 11 show the photomicrographs of 75/25 nylon 6,6/PP blends, modified with 1.47% and 1.84% MA-grafted SEBS mixtures, respectively. Comparing the PTA stained (Fig. 10a and Fig. 11a) to the RuO_4-stained (Fig. 10b and Fig. 11b) photomicrographs, the SEBS segments of the graft tend to form aggregates in the nylon matrix. Most importantly, the nylon–PP interface is almost depleted of SEBS molecules. The reasons for the dramatic difference in morphology of the blends as affected by the level of MA content are given below.

Recall that the system investigated consists of four components: nylon 6,6, nylon-grafted SEBS, non-grafted SEBS and PP. It is postulated that increased maleation draws the grafted SEBS molecules into the nylon phase, leaving fewer SEBS-based molecules available at the nylon–PP interface. Grafted SEBS migrates to the nylon phase, whereas non-maleated SEBS primarily exists in the PP domains. The SEBS segments of the SEBS-nylon graft molecules mix wherever possible with the non-maleated SEBS. A SEBS-rich interface is formed between the PP and nylon phases, with the grafted SEBS on the nylon side and the non-grafted SEBS on the PP side. When the grafted and non-grafted SEBS are present in equal amounts, the interfacial strength and PP dispersion are optimised. Note that the SEBS segments of the SEBS-nylon graft are immiscible with nylon and form aggregates in the PA matrix. Due to the strong propensity of MA-grafted SEBS for reactive copolymerisation with nylon, an increased content of maleation results in the formation of aggregates of the SEBS segments of the graft in the nylon phase. The remaining non-maleated SEBS neither strengthens the interface nor improves the dispersion of the PP particles. To maximise toughening in the 75/25 nylon 6,6/PP blends containing SEBS-*g*-MA, it is therefore proposed that a rubber-toughened nylon matrix, coupled with enhanced compatibility between nylon and PP arising from a well-balanced mixture of MA-grafted and

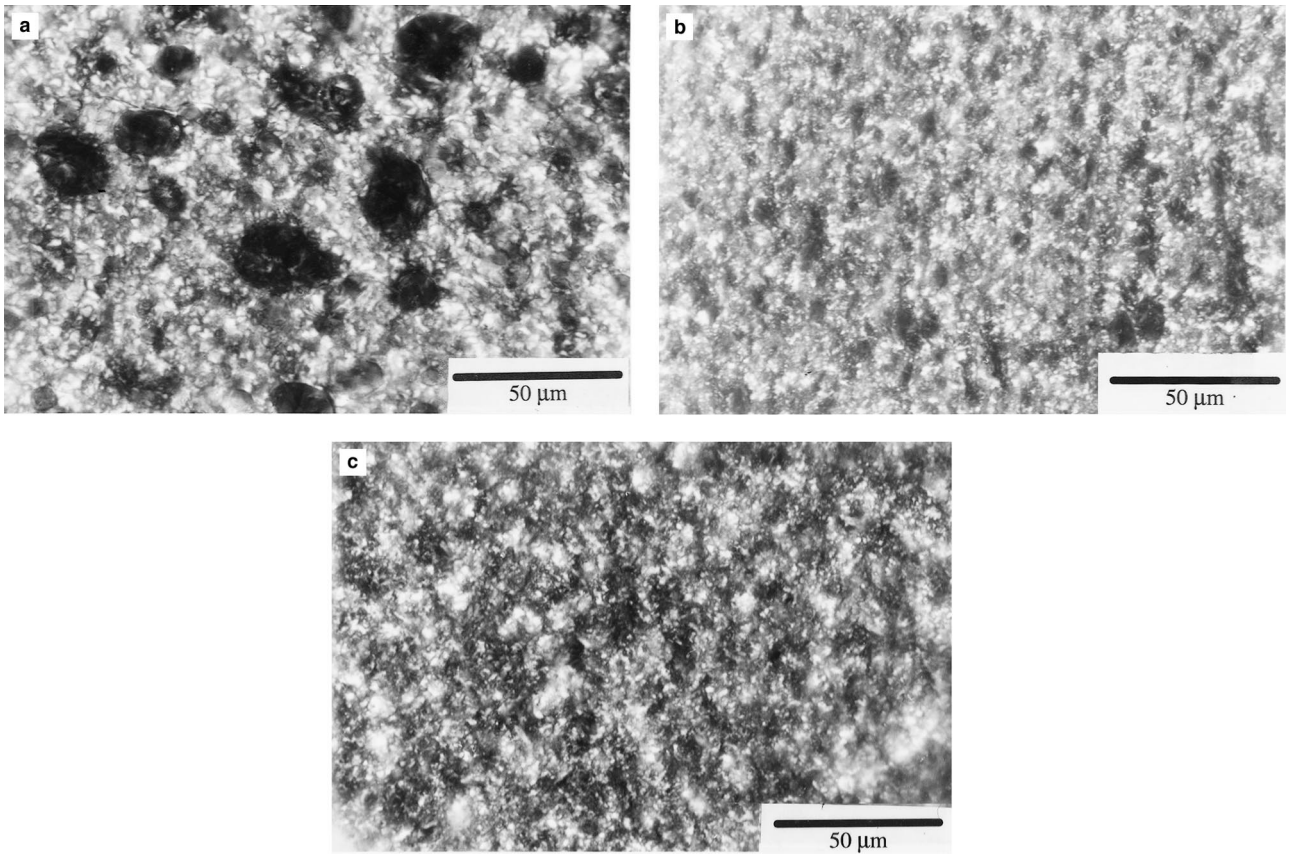

Fig. 7. TOM photomicrographs of 75/25 nylon 6,6/PP blends containing 20 wt% SEBS-*g*-MA: (a) 0.37% MA; (b) 0.74% MA; and (c) 1.84% MA.

non-grafted SEBS which forms the interface, are necessary. Moreover, the morphology of the SEBS-*g*-MA compatibilised interface observed in Figs. 8 and 9 resembles, if not emulates, that of a core-shell rubber. In this case, an embedded SEBS shell encapsulates a hard PP core. It is believed that a core-shell structure like this can provide extremely effective toughening to several rubber-modified blends [22]. The morphology exhibited by the 0.74%-maleated blend, where both grafted and non-grafted SEBS are present in equal amounts, corresponds to maximum fracture toughness and this will be discussed in Section 4. The interpretation of the effects of rubber functionality on the complex morphology of 75/25 nylon 6,6/PP blends containing SEBS-*g*-MA, as discussed above, is summarised in Fig. 12.

4. Mechanical and fracture properties

4.1. Tensile properties

Typical stress–strain curves of different MA content for both 75/25 and 50/50 nylon 6,6/PP blends containing 20 wt% copolymer are shown in Fig. 13. Post-yield failures generally prevail in both systems. But, for the non-maleated blends, the strains at failure are much smaller because of the poor interfacial adhesion between the nylon 6,6 and PP phases. In most other blend compositions, neck formation was noted but it was unstable and the neck continued to thin down until final failure. From the tensile performance of the SEBS-modified nylon 6,6/PP (Fig. 13), the presence of MA evidently provides the minimum level of reactive interface for nylon 6,6 and PP. The tensile strength and ductility of these blends are plotted in Fig. 14. While the tensile strength for the 75/25 nylon 6,6/PP blends continuously increases as MA-grafted SEBS content increases (Fig. 14a), the tensile ductility shows a maximum at 0.74% MA level (Fig. 14b). These results support the proposal that, in the presence of MA, SEBS not only functions as an impact modifier but also as a compatibiliser, whose olefinic mid-block penetrates into the PP domains, while the grafted anhydride functional groups react with the amine-end groups on the nylon. The upper limit of the interfacial strength for the blends exhibiting substantial elongation at break must be higher than the yield stress of the PP particles in order to ascertain plastic deformation followed by debonding in the continuous nylon phase. Fig. 15a shows a microtomed 0.74%-maleated thin section under cross-polarised light of a uniaxially loaded tensile specimen near the point of failure. Debonding of PP particles in the presence of MA evidently occurs after the PP phase has been drawn to some extent by the nylon matrix. In contrast, no evidence of plastic deformation followed by debonding is observed in the 1.84%-maleated

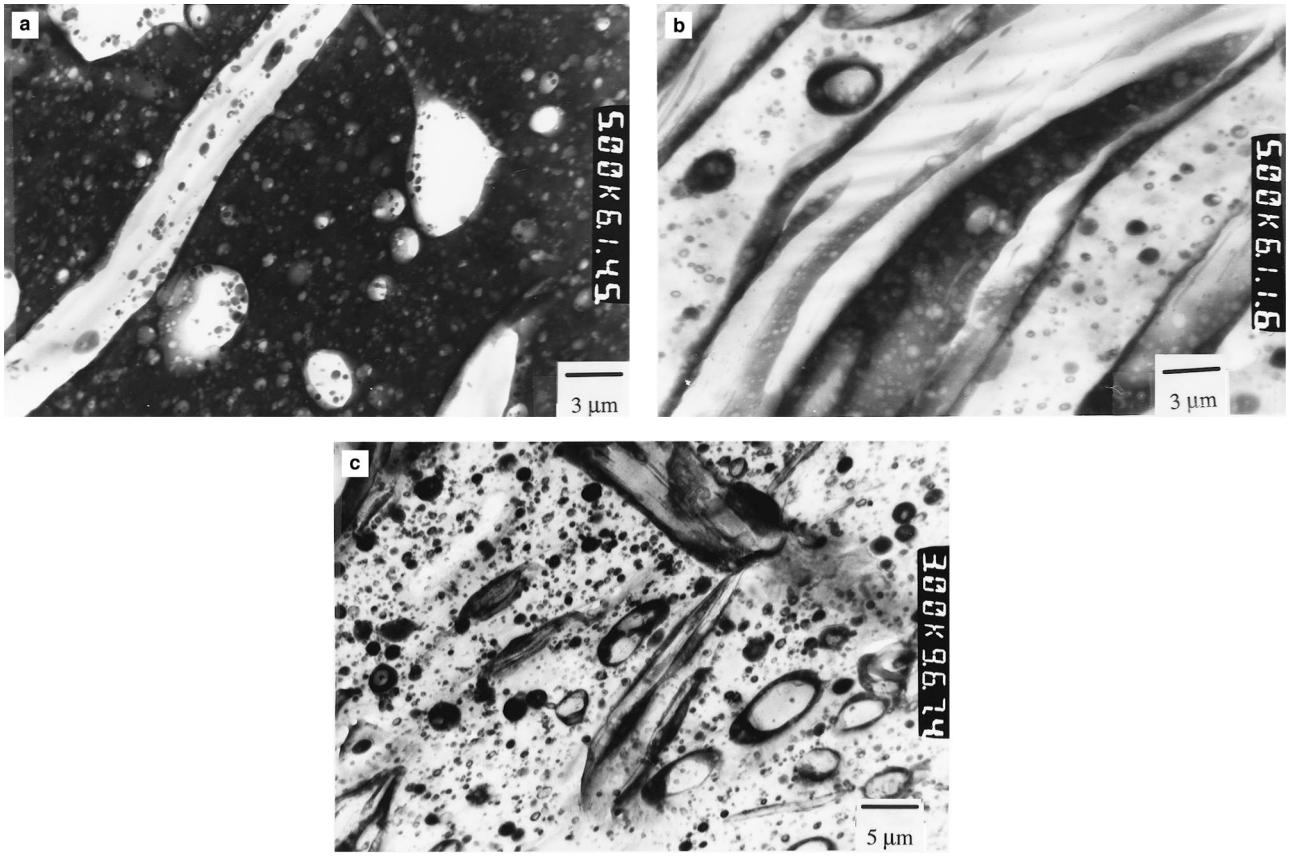

Fig. 8. TEM photomicrographs of 0.37%-maleated 75/25 nylon 6,6/PP blends modified with 20 wt% SEBS-*g*-MA: (a) PTA-stained. Nylon is stained dark; PP and SEBS remain unstained; (b) RuO_4-stained. SEBS is stained dark; nylon and PP remain unstained; and (c) RuO_4-stained at low magnification revealing irregular-shaped PP particles in the nylon-continuous matrix.

blend (Fig. 15b), suggesting reasonably high interfacial tension and hence poor dispersion of PP particles in this blend composition, which is consistent with the microstructures shown in Fig. 11. Note that premature interfacial cracks can be seen on the uniaxially loaded specimen (Fig. 15b).

It is interesting, however, to observe from Fig. 14 that the tensile strength decreases with increasing MA-grafted SEBS content for the 50/50 nylon 6,6/PP blends. Two questions arise when assessing the effect of the particle failure modes on material performance based on the tensile strength

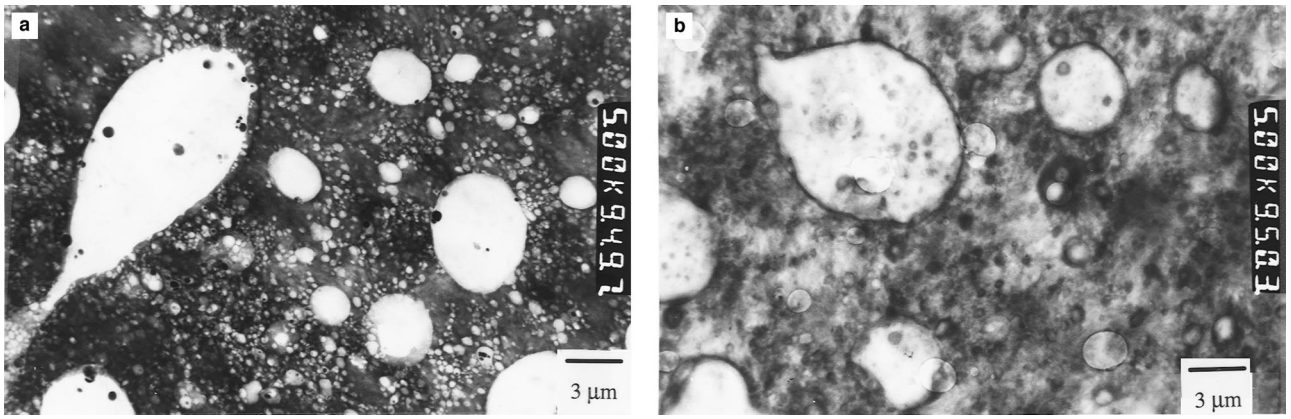

Fig. 9. TEM photomicrographs of 0.74%-maleated 75/25 nylon 6,6/PP blends modified with 20 wt% SEBS-*g*-MA: (a) PTA-stained. Nylon is stained dark; PP and SEBS remain unstained; (b) RuO_4-stained. SEBS is stained dark; nylon is stained dark grey, which is not easily distinguishable from stained SEBS; and PP remains unstained, even after a prolonged period of time (15 h).

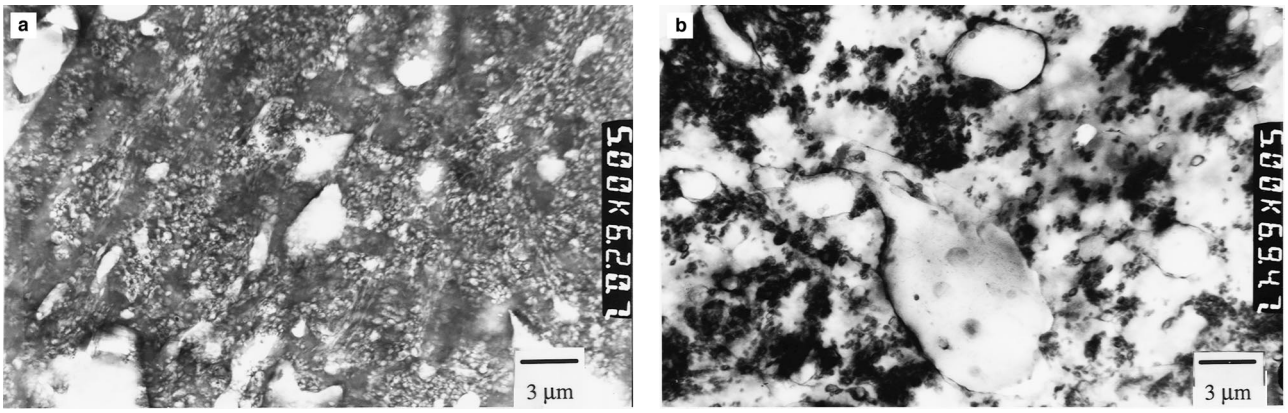

Fig. 10. TEM photomicrographs of 1.47%-maleated 75/25 nylon 6,6/PP blends modified with 20 wt% SEBS-*g*-MA: (a) PTA-stained. Nylon is stained dark; PP remains unstained and some SEBS-commingled nylon phase forms agglomerates adsorbed on the nylon phase; and (b) RuO_4-stained. SEBS is stained dark; nylon and PP remain unstained.

and ductility. First, why does the tensile strength for 75/25 nylon 6,6/PP blends (with 20 wt% SEBS) rise steadily with MA-grafted SEBS whereas the opposite trend occurs for the 50/50 blends? Second, why is there maximum ductility for the 0.74%-maleated blend?

From microscopic observations, maleated styrenic block copolymers are found to migrate to the nylon matrix as the grafted anhydride level increases. In Figs 8–11, it is evident that there exists a migration of SEBS molecules initially from the PP domains to the PP–nylon interface, and subsequently to the nylon phase, where the immiscible SEBS segments form aggregates in the nylon phase. The same process of migration seems to be operative in both a nylon-continuous matrix (75/25 nylon 6,6/PP) and a PP-continuous matrix (50/50 nylon 6,6/PP) owing to the strong propensity of grafted anhydride groups to react with the amine-end groups on nylon. It must be emphasised that the rigid polystyrene blocks in the SEBS can function as reinforcing fillers [7,13] in the continuous phase when tensile properties are evaluated. Increasing the functionality of these styrenic block copolymers by raising the grafted anhydride content automatically introduces a higher dispersion of rigid polystyrene fillers into the nylon-continuous matrix (75/25 nylon 6,6/PP). Simultaneously, this reduces, proportionally, the volume fraction of reinforcing fillers in a PP-continuous matrix, approximately following the grafted/non-grafted SEBS ratio of mixtures, leading to the reverse trend in tensile strength. Further support is given in Fig. 6, showing the very poor interfacial strength between the nylon inclusions and the PP matrix. (The same explanation can be given for the divergent trends of the tensile modulus versus MA content results shown in Fig. 16.)

Comparing the tensile modulus (Fig. 16) with the tensile strength (Fig. 14a) data suggests that enhanced dispersion of polystyrene blocks in the nylon-continuous phase may not be the only factor that controls the strength and stiffness of the 75/25 blends. While the tensile strength shows a positive synergistic increase with MA-grafted SEBS content, the stiffness adheres closely to a linear-additive law. It is shown that, prior to interfacial debonding and final failure, the PP particles are partially drawn (Fig. 15a) and the tensile strength is derived from the stiffer, continuous-nylon matrix

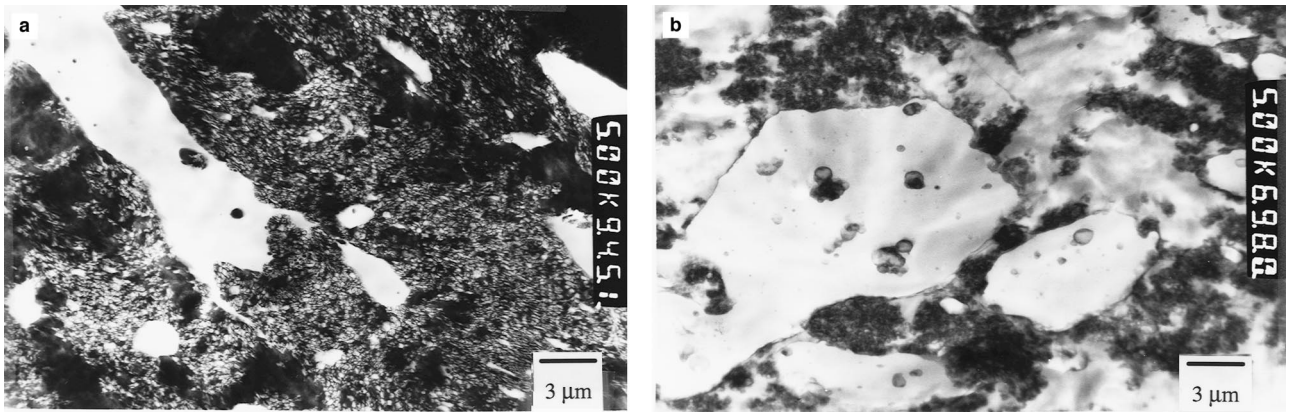

Fig. 11. TEM photomicrographs of 1.84%-maleated 75/25 nylon 6,6/PP blends modified with 20 wt% SEBS-*g*-MA: (a) PTA-stained. Nylon is stained dark; PP remains unstained and some SEBS-commingled nylon phase forms agglomerates adsorbed on the nylon phase; and (b) RuO_4-stained. SEBS is stained dark; nylon and PP remain unstained.

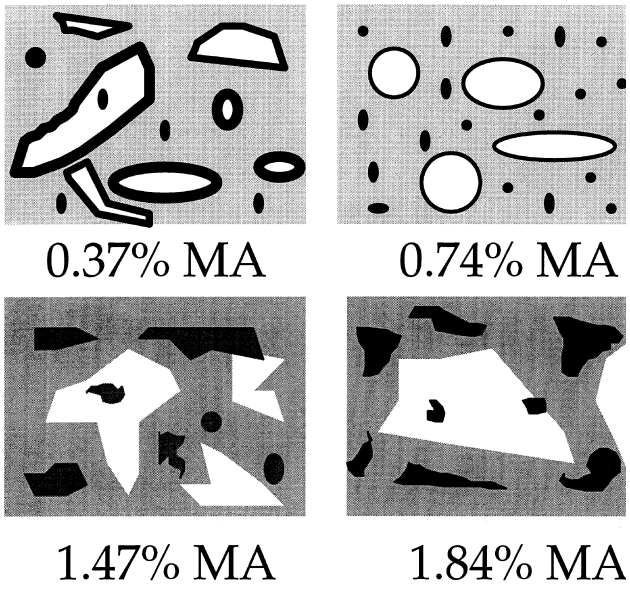

Fig. 12. A schematic that summarizes the micro-morphology of 75/25 nylon 6,6/PP blends modified with 20 wt% SEBS-*g*-MA as revealed by TEM micrographs.

containing sub-micron SEBS inclusions. It is thought that the presence of MA introduces synergistically stronger intermolecular forces in the nylon–SEBS matrices, leading to the tensile strength results in Fig. 14a. The stiffness, however, is obtained from the initial deformation of both PP and nylon and hence varies according to a volume-average relationship as in Fig. 16.

Small and uniformly dispersed particles are more conducive to post-yield plastic deformation. But large, odd-shaped particles often induce brittle failure by creating critical-size defects in the particles and at the particle–matrix interface. For the 0.74%-maleated 75/25 nylon 6,6/PP blend, the PP inclusions are finely dispersed and sub-micron SEBS inclusions are well distributed in the nylon-continuous matrix (Fig. 9). Consequently, premature failure caused by interface debonding or particle fracture is discouraged, leading to a maximum elongation-to-break, as shown in Fig. 14b.

4.2. Fracture toughness results

Increasing interest has been generated in recent years in fracture toughness characterization of novel polymer blends [33–38] using non-linear elastic fracture mechanics parameters. In contrast to the geometry-dependent, but standardized, impact test [39], the primary advantage of employing fracture mechanics parameters in assessing toughness is a unique material property at the onset of crack growth. In this study, it was found that the fracture toughness of nylon 6,6/PP/SEBS-*g*-MA blends shows an unambiguous dependence on the rubber functionality given by the grafted MA content. In a nylon-rich matrix, it is observed that the variation of J_C with MA (Fig. 17) closely matches that of the tensile

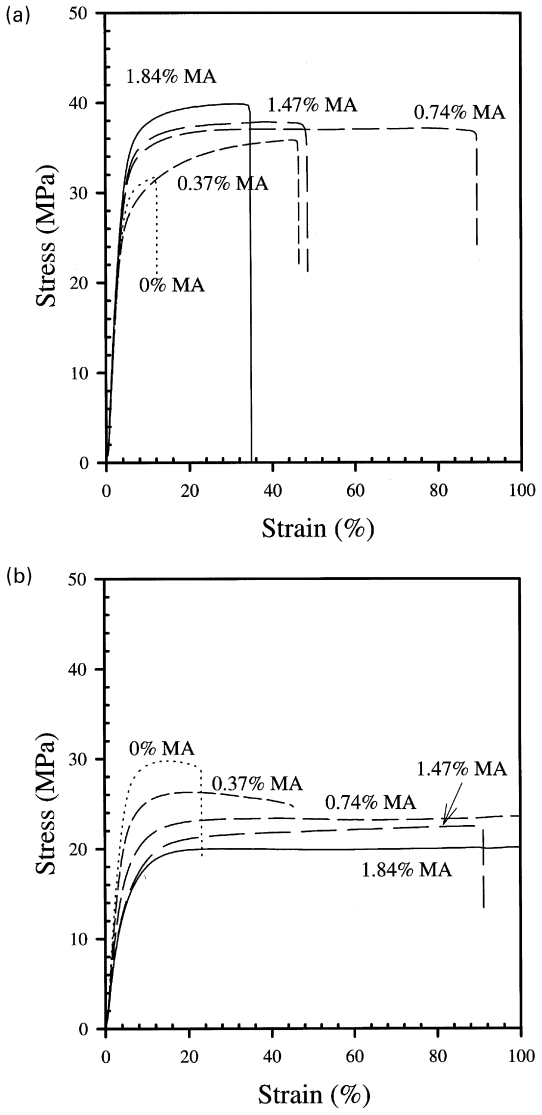

Fig. 13. Representative stress–strain curves of: (a) 75/25; and (b) 50/50, nylon 6,6/PP blends containing SEBS-*g*-MA.

ductility (Fig. 14b). J_C reaches a maximum value at 0.74% MA content, with an optimal combination of tensile strength and ductility. Recall that, at this MA level, the blend has well-dispersed SEBS inclusions in the continuous nylon phase (Fig. 9a), effectively toughening the matrix. In addition, there are PP inclusions surrounded by SEBS fringes forming a 'core-shell' morphology (Fig. 9b), as first suggested by Rösch and Mülhaupt [7]. The dispersed SEBS/PP inclusions allow plastic yielding, followed by debonding and subsequent matrix deformation (Fig. 15a) to take place, giving rise to maximum ductility (Fig. 14b). Thus the fracture toughness is also maximised. In those other blends in which diminished fracture toughness is observed when the MA-grafted SEBS content is either too low or too high, this is caused by the poor dispersions of PP phase in the SEBS-modified nylon matrix resulting in premature cracks. (See for example Fig. 15b). All these results point to the fact that 75/25 nylon 6,6/PP blends can be tailored to

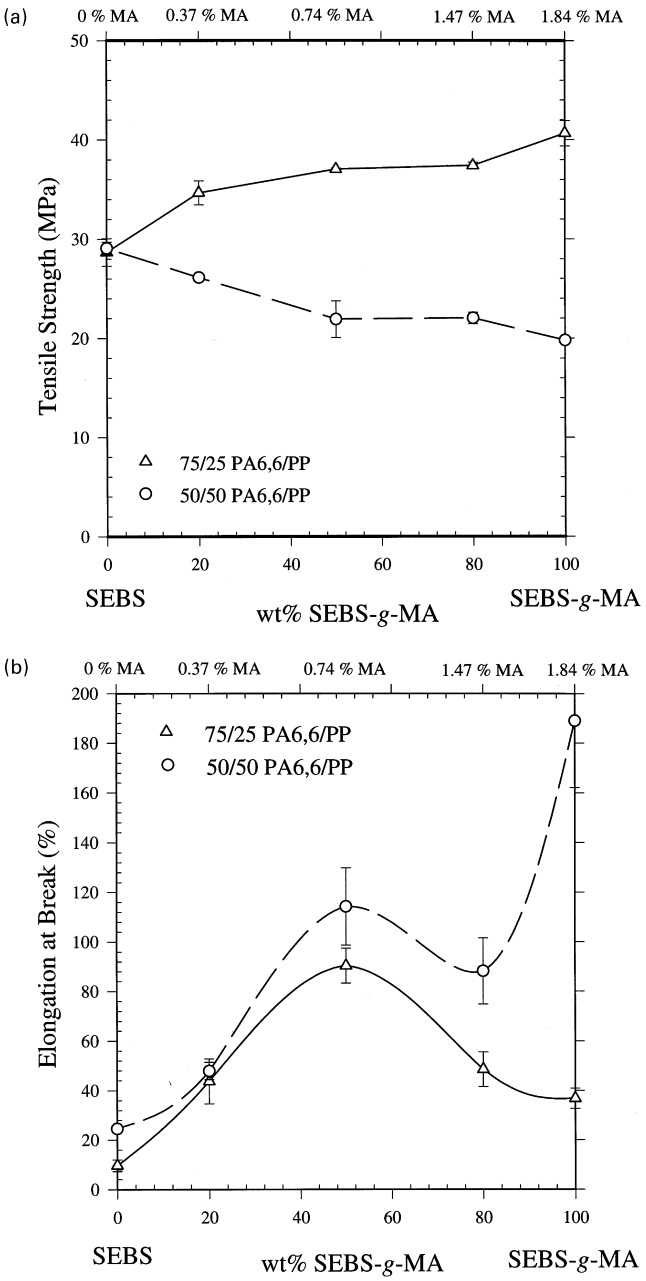

Fig. 14. Effect of rubber functionality on: (a) tensile strength; and (b) elongation at break, of nylon 6,6/PP blends modified with SEBS-*g*-MA.

possess high fracture toughness with good tensile strength and high stiffness by properly controlling the phase morphology using SEBS-*g*-MA. Tensile ductility seems to be the predominant factor in controlling the fracture toughness in these 75/25 blends.

A transition from a nylon-continuous to a PP-continuous morphology generally decreases the crack resistance. Fig. 17 confirms that the 50/50 nylon 6,6/PP blends containing SEBS-*g*-MA have lower J_C toughness values compared with the 75/25 system (except for the non-maleated and 1.84%-maleated blends). J_C decreases with the MA content up to 1.47% and then increases slightly at 1.84%. This trend

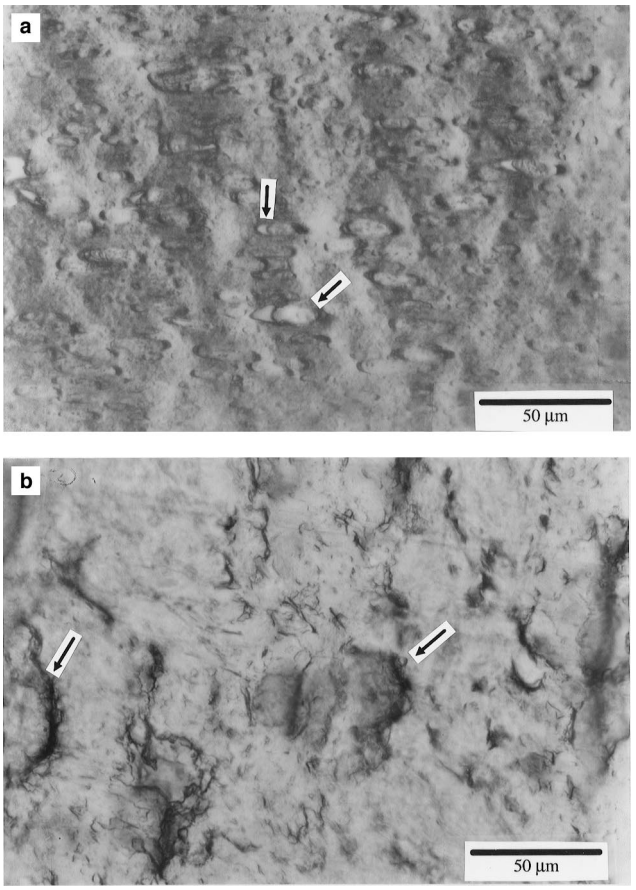

Fig. 15. TOM photomicrographs show: (a) plastic debonding in 0.74%-maleated; and (b) premature interfacial cracks in 1.84%-maleated uniaxially loaded tensile specimens, from 75/25 nylon 6,6/PP blends containing SEBS-*g*-MA.

seems to run parallel to the tensile strength (Fig. 14a) for MA levels less than 1.47%, but at 1.84% MA the high ductility has stopped the decreasing trend and improved the fracture toughness.

5. Conclusions

1. The micro-morphology of nylon 6,6/PP blends modified by SEBS-*g*-MA of different anhydride content was studied using microscopic techniques (SEM, TOM and TEM). It was found that the size of dispersed second phase particles decreased as the MA-grafted SEBS content increased. SEBS inclusions in the nylon-rich matrices appeared to disperse in the nylon matrix and at the nylon–PP interface for blends with 0.74% or less MA content. However, these SEBS inclusions form aggregates in the nylon phase for blends at higher MA levels. An optimised morphology for maximum fracture–mechanical properties was found to exist in the 0.74%-maleated blend.
2. Plastic deformation followed by debonding of PP

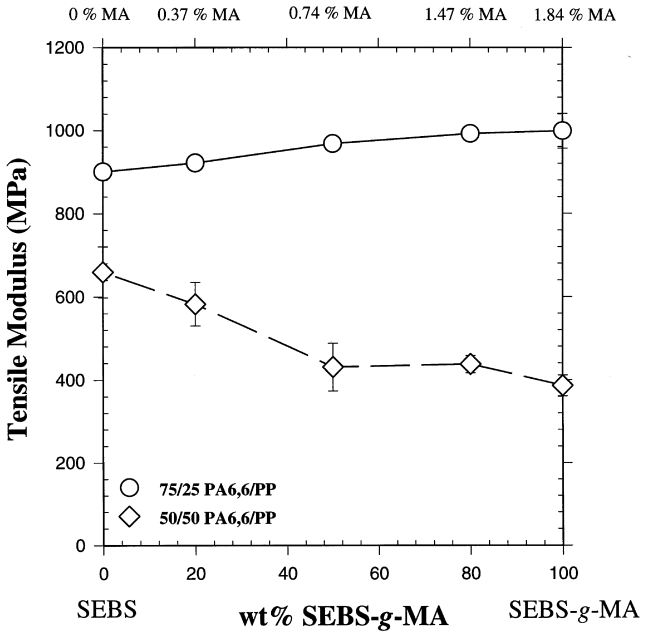

Fig. 16. Effect of rubber functionality on tensile moduli of 75/25 and 50/50 nylon 6,6/PP blends containing SEBS-*g*-MA.

inclusions evidently occurred in blends with high elongation at break, whereas premature interfacial cracks prevailed in blends with low ductility. It was suggested that the ability of the dispersed phase to plastically deform and debond, coupled with an effectively toughened continuous matrix, could impart a high fracture toughness in multiphase polymer blends.

3. Tensile strength and stiffness increased with MA-grafted SEBS content in the 75/25 nylon 6,6/PP blends but an opposite trend occurred in the 50/50 nylon 6,6/PP blends. Phase inversion occurred in the 50/50 system where PP became the continuous phase. Migration of the functionalised styrenic block copolymers from the PP phase to the nylon phase occurred in both systems. An intrinsic strengthening behaviour by the rigid polystyrene blocks of the functionalised SEBS copolymers was believed to be the cause for stiffening in the nylon-rich blends and weakening in the PP-continuous blends. It was concluded that nylon inclusions in SEBS-modified PP matrices did not provide any reinforcement effect because of the poor interfacial adhesion.
4. The fracture toughness of the nylon 6,6/PP blends containing 20 wt% SEBS was dramatically altered by the grafted MA level and intimately related to the phase morphology and microstructures. It was suggested that the tensile strength and ductility are two important factors that affect the fracture toughness of the nylon 6,6/PP blends. While tensile ductility controls J_C of the 75/25 nylon 6,6/PP blends, tensile strength appears to control J_C of the 50/50 nylon/PP blends.

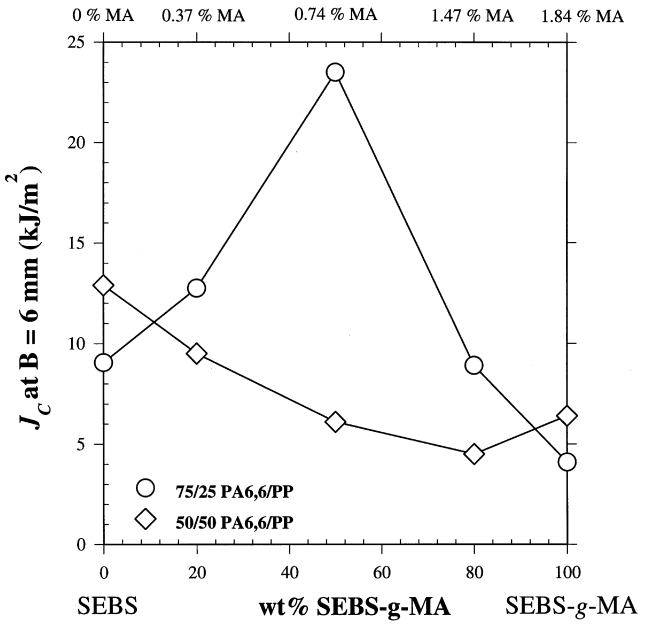

Fig. 17. Effect of rubber functionality on *J*-integral fracture initiation toughness of 75/25 and 50/50 nylon 6,6/PP blends containing SEBS-*g*-MA.

Acknowledgements

The authors would like to thank the Australian Research Council (ARC) for the continuing support of this polymer blends project. S.-C. Wong acknowledges the award of a Postgraduate Research Scholarship funded by the ARC and tenable at the University of Sydney. Monsanto Company supplied the nylon 6,6 resins; Shell Chemical provided the impact modifiers; and ICI Australia the PP resins. Thanks are also due to the Electron Microscope Unit at the University of Sydney for providing access to its characterisation facilities. Finally, the referee's constructive comments on the factors affecting morphology of the blends have considerably improved the quality of the paper and this is much appreciated.

References

[1] Gelles R, Modic M, Kirkpatrick J. Modification of engineering thermoplastics with functionalised styrenic block copolymers. In: Proc. of the Soc. Plast. Engr. 46th Annual Technical Conference. ANTEC'88, Society of Plastics Engineers, Brookfield, CT, 1988:513.
[2] Gilmore D, Modic MJ. Engineering polymer blends with styrenic block copolymers. In Proc. of the Soc. Plast. Engr. 48th Annual Technical Conference. ANTEC'90, Society of Plastics Engineers, Brookfield, CT, 1990:1228.
[3] Modic MJ. Compatibilization of polyamide/polyolefin blends with functionalized styrenic block copolymers. In: Proc. of the Soc. Plast. Engr. 51st Annual Technical Conference. ANTEC'93, Society of Plastics Engineers, Brookfield, CT, 1993:205.
[4] Modic MJ, Pottick LA. Polym Engng Sci 1993;33:819.
[5] Holsti-Miettinen RM, Seppälä JV, Ikkala OT, Reima IT. Polym Engng Sci 1993;34:395.
[6] Gupta AK, Purwar SN. J Appl Polym Sci 1984;29:3513.
[7] Rösch J, Mülhaupt R. Polym Bull 1994;32:697.

[8] Rösch J. Polym Engng Sci 1995;35:1917.
[9] Oshinski AJ, Keskkula H, Paul DR. Polymer 1992;33:268.
[10] Oshinski AJ, Keskkula H, Paul DR. Polymer 1992;33:284.
[11] Gonzalez-Montiel A, Keskkula H, Paul DR. Polymer 1995;36:4587.
[12] Gonzalez-Montiel A, Keskkula H, Paul DR. Polymer 1995;36:4605.
[13] Gonzalez-Montiel A, Keskkula H, Paul DR. Polymer 1995;36:4621.
[14] Gonzalez-Montiel A, Keskkula H, Paul DR. J Polym Sci B Polym Phy 1995;33:1751.
[15] Duvall J, Sellitti C, Topolkaraev V, Hiltner A, Baer E, Myers C. Polymer 1994;35:3948.
[16] Borggreve RJM, Gaymans RJ, Schuijer J, Ingen Housz JF. Polymer 1987;28:1489.
[17] Bucknall CB, Karpodinis A, Zhang XC. J Mater Sci 1994;29:3377.
[18] Guild FJ, Young RJ. J Mater Sci 1989;24:298.
[19] Guild FJ, Young RJ. J Mater Sci 1989;24:2454.
[20] Wu S. Polymer 1985;26:1855.
[21] Turley SG, Keskkula H. Polymer 1980;21:466.
[22] Parker DS, Sue H-J, Huang J, Yee AF. Polymer 1990;31:2267.
[23] Yee AF, Li D, Li X. J Mater Sci 1993;28:6392.
[24] Mai Y-W, Powell P. J Polym Sci B Polym Phy 1991;29:785.
[25] Martinez-Salazar J, Cannon CG. J Mater Sci Lett 1984;3:693.
[26] Trent JS, Scheinbeim JI, Couchman PR. Macromolecules 1983;16: 589.
[27] Wong S-C, Mai Y-W. On novel PA6,6/PP/SEBS-*g*-MA blends. In: Miyano Y, Yamabe M, editors. Proc. 5th Japan International SAMPE Symposium. Tokyo: Society for the Advancement of Materials and Process Engineering, 1997, Yokohama, Japan. Tokyo Big Sight 28–31 October 1997:89–94.
[28] Wu S. J Appl Polym Sci 1988;35:549.
[29] Wu S. Polym Engng Sci 1987;27:335.
[30] Borggreve RJM, Gaymans RJ, Eichenwald HM. Polymer 1989;30:78.
[31] Borggreve RJM, Gaymans RJ. Polymer 1989;30:63.
[32] Borggreve RJM, Gaymans RJ, Schuijer J. Polymer 1989;30:71.
[33] Wu J-S, Mai Y-W, Cotterell B. J Mater Sci 1993;28:3373.
[34] Wu J-S, Mai Y-W. Polym Engng Sci 1996;36:2275.
[35] Lu ML, Chang FC. J Appl Polym Sci 1995;56:1065.
[36] Lu ML, Chiou KC, Chang FC. J Appl Polym Sci 1996;62:863.
[37] Lu ML, Chang FC. Polymer 1995;36:4639.
[38] Lu ML, Chiou KC, Chang FC. Polymer 1996;37:4289.
[39] Jancar J, Dibenedetto AT. Polym Engng Sci 1994;34:1799.